Materials Science in Semiconductor Processing 135 (2021) 106045

Contents lists available at ScienceDirect

Materials Science in Semiconductor Processing

journal homepage: www.elsevier.com/locate/mssp

Comparison of n and p type Si-based Schottky photodiode with interlayered Congo red dye

Adem Kocyigit [a,b,*], Mehmet Yilmaz [c,d,**], Sakir Aydogan [e], Ümit İncekara [f,g], Hatice Kacus [e]

[a] Department of Electrical and Electronics Engineering, Engineering Faculty, Igdir University, 76000, Igdir, Turkey
[b] Department of Electronics and Automation, Vocational High School, Bilecik Şeyh Edebali University, 11230, Bilecik, Turkey
[c] Advanced Materials Research Laboratory, Department of Nanoscience and Nanoengineering, Graduate School of Natural and Applied Sciences, Ataturk University, 25240, Erzurum, Turkey
[d] Department of Science Teaching, K.K. Education Faculty, Ataturk University, 25240, Erzurum, Turkey
[e] Department of Physics, Science Faculty, Atatürk University, 25240, Erzurum, Turkey
[f] Department of Basic Sciences, Science Faculty, Erzurum Technical University, 25240, Erzurum, Turkey
[g] Department of Biology, Science Faculty, Atatürk University, 25240, Erzurum, Turkey

ARTICLE INFO

Keywords:
Photodiodes
Metal-semiconductor devices
Schottky
Congo red
Responsivity

ABSTRACT

We synthesized a thin film of Au nanoparticles-decorated Congo red (CR) dye on both *n*-Si and *p*-Si substrates by the spin coating technique. UV–Vis spectrometer was used to determine the absorbance and band gap of the CR film. Transmission electron microscope (TEM) was used to assess the distribution of Au nanoparticles on the CR dye film. Then, the metal-semiconductor devices were fabricated by evaporation of Co metal and Al ohmic contacts on the front and back surfaces of the CR film-covered substrates, respectively. Thus, Co/CR:Au/n-Si and Co/CR:Au/p-Si Schottky photodiodes were fabricated and characterized by *I–V* measurements under dark and various light power illumination intensities at room temperature. The devices exhibited good rectifying behaviors and low barrier heights. Various diode parameters such as ideality factor, barrier height, and series resistance values were calculated and compared for the two fabricated photodiodes. The Co/CR:Au/n-Si and Co/CR:Au/p-Si devices exhibited good photodiode and photodetector properties. Various detection parameters revealed that the obtained devices can be improved for optoelectronic applications.

1. Introduction

Organic materials have received increasing interest because of their environmental compatibility, low cost, flexibility, and safe for human health [1]. Various organic materials have been used for technological applications such as solar cells, photodetectors, LEDs, and FET [2,3]. They can be used for photodiode applications to improve the performance of device [4]. Among the organic materials, 3,3′-[(1,1′, -biphenyl)-4,4′-diyl)bis(4-amino-1 amino naphthalene sulphonic)] or Congo red is a type of anionic organic dye with $C_{32}H_{22}N_6Na_2O_6S_2$ chemical formula, and it is used for light-induced photoisomerization and reversible optical data storage [5].

Photodiodes convert light into an electrical signal when the light hits the photodiode surface, but their operation differs from that of normal diodes at reverse biases. In dark conditions, a photodiode behaves as a normal diode to stop the current at reverse biases [6,7]. However, light increases the reverse bias current depending on the power intensity of the incident light. Most of the photodiodes are designed as PIN diodes from a *p*-type region and an *n*-type region with an intrinsic semiconductor between them. However, both the *p*-region and *n*-region decrease reaction time of the photodiode [8]. A Schottky photodiode has a low response time because of lacking of one more diffusion tail. Moreover, the efficiency of the photodiodes can be improved by adding plasmonic nanoparticles into the photodiodes as well as organic layers [9,10].

Organic materials can be used for photodiode and photodetector applications because of the increasing use of light-dependent carriers as an interfacial layer in the interface of the device [11,12]. In the present study, we used Congo red dye with Au nanoparticles as an interfacial layer between the Co and Si substrates, and the Co/CR:Au/n-Si and

* Corresponding author. Department of Electrical Electronic Engineering, Engineering Faculty, Igdir University, 76000, Igdir, Turkey.
** Corresponding author. Advanced Materials Research Laboratory, Department of Nanoscience and Nanoengineering, Graduate School of Natural and Applied Sciences, Ataturk University, 25240, Erzurum, Turkey.
E-mail addresses: kocyigita58@gmail.com (A. Kocyigit), yilmazmehmet32@gmail.com (M. Yilmaz).

https://doi.org/10.1016/j.mssp.2021.106045
Received 19 February 2021; Received in revised form 22 June 2021; Accepted 26 June 2021
Available online 27 July 2021

Co/CR:Au/p-Si photodiodes were fabricated. *I–V* measurements were performed on the photodiodes to characterize the electrical properties under various illumination intensities.

2. Experimental details

Congo red dye and Au nanoparticles were purchased from Sigma-Aldrich and used directly without any further purification. The Congo red dye was dissolved in water, and Au nanoparticles were added to the Congo red solution to obtain a mixture of Au nanoparticles with Congo red. Both *n*-Si and *p*-Si substrates, which had carrier concentration of 7.5 $\times$ 10^{16} cm^{-3}, 1–10 Ω-cm resistivity, and 400-μm thick, were sliced into 1 cm^2 pieces and cleaned with various alcohols according to RCA processes described previously [13]. The Al ohmic contacts were evaporated on the back or unpolished surfaces of the substrates, and the wafers were transferred immediately to a nitrogen-filled furnace for annealing only 5 min. Then, the Congo red solution was coated on the front surfaces of the Si substrates at 3000 rpm and 30 s by a spin coater. Finally, the Co metal was evaporated on the Congo red films by a thermal evaporator by using an array of mask with 7.85 $\times$ 10^{-3} cm^2 opening areas. Thus, the Co/CR:Au/n-Si and Co/CR:Au/p-Si photodiodes were obtained. Fig. 1 shows the schematic illustration of the fabricated devices.

PerkinElmer Lambda 45 UV–Vis spectrometer was used to acquire absorption spectra of the CR film. TEM image of the Au nanoparticles-decorated CR dye was acquired by Hitachi HighTech HT7700. The photodiodes were characterized by *I–V* measurements under dark and various light power illumination intensities. Keithley 2400 was used as an *I–V* sourcemeter, and Sciencetech solar simulator (AM1.5 G or solar spectrum) was used to illuminate the photodiodes for various light power intensities from 100 mW to 400 mW by 50 mW interval per cm^2 surface area.

3. Results and discussion

The optical properties of the CR films were investigated by UV–Vis spectroscopy. The variation in the optical absorbance against wavelength is shown in Fig. 2a. The absorbance graph reveals that the CR film has a narrow band structure with an absorption coefficient in the range of 5 cm^{-1}. In previous studies, the optical band gap nature of the materials was tested using both experimental and theoretical methods, which indicated the importance of optical band gap characterization [14,15]. Hence, the Tauch method can be compared with the absorption coefficient and photon energy obtained from absorption spectra. We used it to determine the nature of the optical band gap of the CR film. For noncrystalline materials, the relationship between absorption coefficient and photon energy is as follows [16]:

$$\alpha(h\nu) = A(h\nu - E_g)^s \quad (1)$$

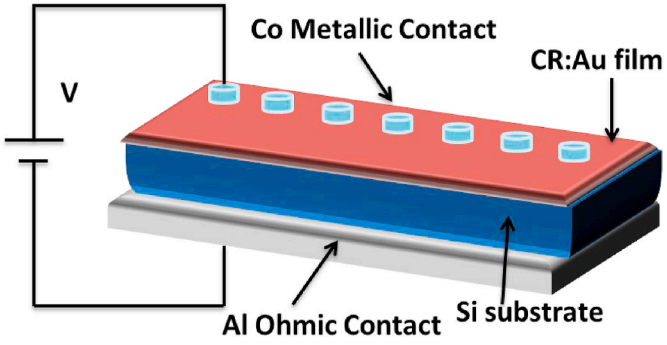

Fig. 1. Schematic illustration of the Co/CR:Au/n-Si and Co/CR:Au/p-Si photodiodes.

where α is the absorption coefficient, $h\nu$ represents photon energy, A is a constant, E_g is the optical bandgap, and s indicates the nature of transition. When the value of s is ½, it shows direct transition, while when the value of s is 2, it shows indirect transition [17]. These correspond to the cases where the electronic momentum is conserved and not conserved in the transitions, respectively. In this context, the nature of transition is very important for optical materials. The easiest way to determine whether the optical transition is direct or indirect is to plot the $(\alpha h\nu)^2$ versus $h\nu$ and $(\alpha h\nu)^{0.5}$ versus $h\nu$. Here, it is necessary to observe the linear part that indicates the optical transition in the plot. While Fig. 2b clearly shows optical transformation of this condition, while Fig. 2c shows a nonlinear component. Therefore, the CR film studied in this study has direct optical transition with a 4.07 eV optical band gap.

Furthermore, the presence of Au nanoparticles in the synthesized CR layer was demonstrated using TEM measurement. TEM image of the Au nanoparticles-decorated CR layer are shown in Fig. 2d. Au nanoparticles aggregated and exhibited a nonhomogeneous distribution as observed in TEM images The dimensions of Au NPs were also examined, and the results were shown as embedded in Fig. 2d as a histogram graph. The histogram graph revealed that Au NPs exhibited a Gaussian distribution, and the average size of Au NPs was determined to be approximately 7.58 nm.

I–V characteristics of the Co/CR/*n*-Si and Co/CR/*p*-Si photodiodes are shown in Fig. 3a and b, respectively, to understand the effect of Au nanoparticles on the photodiodes. The photocurrent at reverse biases increased with 100 mW light power intensity to almost 100-fold for the Co/CR/*n*-Si, but it did not change much for the Co/CR/*p*-Si photodiode. Furthermore, a large current shift was clearly observed for the Co/CR/*n*-Si photodiode. These differences can be attributed to semiconductor and metal types. The work functions of the Co element, *n*-type Si, and *p*-type Si were 5 eV, 4.05 eV and 5.15 eV, respectively [18]. The contact between the Co and *n*-type Si can easily be composed of rectifying contact, but the Co and *p*-type Si contact cannot. The CR layers and the native oxide layer on the Si substrate can help to compose rectifying contact for Co and *p*-Si contact [19]. For Au nanoparticles added to the CR layer, both the Co/CR:Au/*n*-Si and Co/CR:Au/*p*-Si photodiodes exhibited better performance than the CR interlayers alone. This can be attributed to the plasmonic behaviors of Au nanoparticles due to efficient trapping of incident light and increase in photocurrent for optoelectronic devices [20–22].

I–V characteristics of the Co/CR:Au/*n*-Si and Co/CR:Au/*p*-Si photodiodes under dark and various light power intensities are shown in Fig. 4a and b, respectively. The obtained photodiodes exhibited normal diode characteristics due to current passage at forward biases and current blockage at reverse biases [23]. When the photodiodes were exposed to the light, the current increased at reverse biases because of photodiode characteristics depending on light power intensity. The Co/CR:Au/*n*-Si photodiode showed a lower dark reverse current and higher photocurrent at a certain light power than the Co/CR:Au/*p*-Si photodiode due to close work functions of *n*-Si and Co element. The forward bias current of the Co/CR:Au/*p*-Si photodiode did not change so much with increasing light power, but it increased for the Co/CR:Au/*n*-Si photodiode. These differences in current for forward and reverse biases can be attributed to the work function differences of *n*-type and *p*-type substrates. The reverse biases of the Co/CR:Au/*n*-Si and Co/CR:Au/*p*-Si photodiodes increased with the increase in reverse biases under dark. However, increasing light caused a flat profile by the changing the current at reverse biases. Moreover, light exposure caused a shift in the minimum current values to the forward bias region owing to increasing charge carrier in the interface of the photodiodes. Thus, the devices exhibited photovoltaic behavior [24].

I–V characteristics of the Co/CR:Au/*n*-Si and Co/CR:Au/*p*-Si photodiodes were used to calculate various diode parameters such as ideality factor (n) and barrier height (ϕ_b) as well as series resistance (R_s). First,

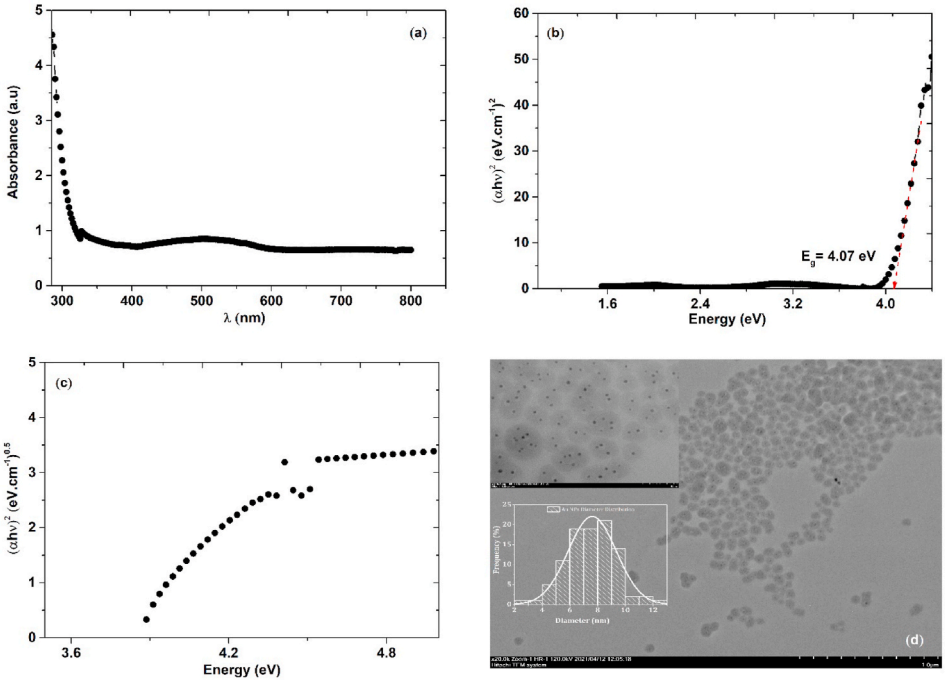

Fig. 2. a) Optical absorbance spectra, b) $(\alpha h\nu)^2$ versus energy c) $(\alpha h\nu)^{0.5}$ versus energy plots of the CR film, and d) TEM image of Au nanoparticles-decorated CR structures.

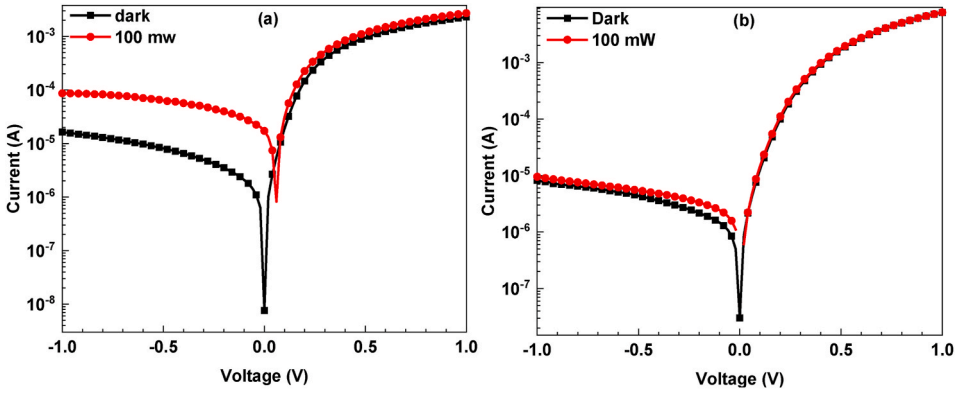

Fig. 3. Semi-logarithmic *I–V* characteristics of the a) Co/CR/*n*-Si and b) Co/CR/*p*-Si photodiodes under dark and 100 mW/cm^2 light power intensity.

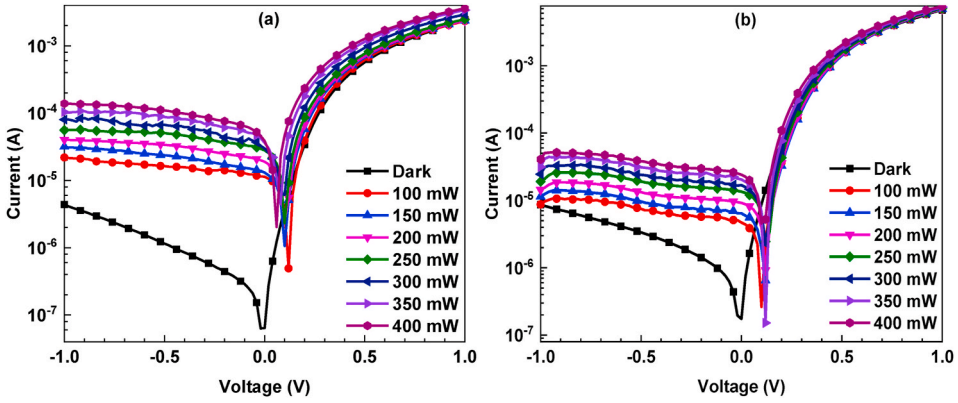

Fig. 4. Semi-logarithmic *I–V* characteristics of the a) Co/CR:Au/*n*-Si and b) Co/CR:Au/*p*-Si photodiodes for various light power intensities.

Table 1
Various diode parameters of the Co/CR:Au/*n*-Si and Co/CR:Au/*p*-Si photodiodes.

Photodiode	Saturation Current (I_o)	n (I–V) –	n Cheung –	Φ_b (I–V) (eV)	Φ_b Cheung (eV)	Φ_b Norde (eV)	R_s Cheung (kΩ ($H(I)$))	R_s Cheung ((kΩ ($d\ln(I)$))	R_s Norde (kΩ)
Co/CR:Au/*n*-Si	9.10×10^{-7}	1.42	1.42	0.65	0.68	0.72	0.61	0.68	0.64
Co/CR:Au/*p*-Si	4.37×10^{-7}	1.39	1.39	0.64	0.64	0.67	0.21	0.20	0.31

the thermionic emission theory was employed to obtain the n and ϕ_b values for dark and various light illumination power intensities. The calculated n and ϕ_b values for the Co/CR:Au/*n*-Si and Co/CR:Au/*p*-Si photodiodes under dark are listed in Table 1. The n and ϕ_b values are close to each other for both photodiodes. Fig. 5a and b displays a light intensity-dependent profile of the n and ϕ_b values for the Co/CR:Au/*n*-Si and Co/CR:Au/*p*-Si photodiodes. While the ideality factor values increased with the increase of light power intensity, the barrier height values decreased for both Co/CR:Au/*n*-Si and Co/CR:Au/*p*-Si photodiodes. Both the ideality factor and barrier height values were slightly higher for Co/CR:Au/*n*-Si than for Co/CR:Au/*p*-Si due to the work function differences of the *n*-type and *p*-type Si substrates.

The shunt and series resistance are important parameters to affect the electrical behaviors of the photodiodes [25]. While the shunt resistance (R_{sh}) value of a diode remains constant at a certain reverse bias, the R_s value is determined at the high forward bias for constant values of the junction resistance (R_j) [26]. Fig. 6a and b shows the R_j versus voltage plots of the Co/CR:Au/*n*-Si and Co/CR:Au/*p*-Si photodiodes depending on the various light power illumination intensities. For the Co/CR:Au/*n*-Si photodiode, increased up to a certain value from 0.5 V to 0 for various light power intensities and stayed almost constant toward higher reverse biases. For the Co/CR:Au/*p*-Si photodiode, the R_j values remained constant at higher forward biases and increased suddenly at around 0. Both devices exhibited peaks, and the intensities of the peaks or R_{sh} values decreased with increasing light power due to increasing charge carriers. While the R_{sh} values of the photodiodes are around 10^4–10^6 Ω, the R_s values are about 200–300 Ω for both devices. These values are suitable for this type of photodiode, and the photodiodes can be used for optoelectronic applications [27].

The Norde method was used to confirm the obtained diode parameter results from the thermionic emission theory [28]. The Norde function plots of the Co/CR:Au/*n*-Si and Co/CR:Au/*p*-Si photodiodes in dark are shown in Fig. 7a and b, respectively. The photodiodes exhibited a normal Norde function profile. The calculated barrier height and series resistance values are shown in Table 1. The calculated parameters are in good agreement with those from the thermionic emission ideality factor and barrier height values.

Another technique to confirm the calculated parameters is the Cheung method [29]. There are two Cheung functions: $dV/d(\ln I)$ and $H(I)$, and they exhibit straight lines when the functions are plotted against current. These plots enable to determine the n, Φ_b, and two R_s values. The determination of the diode parameters has been reported previously [30]. The Cheung plots of the Co/CR:Au/*n*-Si and Co/CR:Au/*p*-Si photodiodes for dark condition are shown in Fig. 8a and b, respectively. The Cheung functions exhibited good linearity for both photodiodes. The determined n, Φ_b, and two R_s values are shown in Table 1 for both photodiodes. The obtained diode parameters are in harmony with the other techniques and confirm the correction of the results [31].

The responsivity (R) of a photodiode is an important parameter because it shows the input-output gain of the device [32]. The R–V plots of the Co/CR:Au/*n*-Si and Co/CR:Au/*p*-Si photodiodes depending on the increasing light power intensity are illustrated in Fig. 9a and b, respectively. The responsivity values increased with the increase of light power and reverse biases for both photodiodes. The responsivity values of the Co/CR:Au/*n*-Si photodiode was almost four times higher than that of the Co/CR:Au/*p*-Si photodiode. There was a sudden decrease in the R values at around −1 V for the Co/CR:Au/*p*-Si photodiode due to slow change in the photocurrent with increasing light power intensity.

The various detection parameters as well as rectifying ratio (RR) of the Co/CR:Au/*n*-Si and Co/CR:Au/*p*-Si photodiodes with changing light power intensity were investigated. The rectifying ratio (for a certain voltage value), responsivity, and specific detectivity formulas are given as follows:

$$RR = \frac{I_{forward}}{I_{reverse}} \tag{1a}$$

$$R = \frac{I_p}{PA} \tag{2}$$

$$D^* = R\sqrt{\frac{A}{2qI_{dark}}} \tag{3}$$

where I_p exhibits photocurrent, P is incident power density, and A is the effective detector area.

Fig. 10a, b, c, and d show the rectifying ratio (RR), photocurrent, responsivity, and specific detectivity changes of the photodiodes depending on the light power intensity, respectively. The RR values were decreased for both the Co/CR:Au/*n*-Si and Co/CR:Au/*p*-Si photodiodes with increasing light power. The RR values of the Co/CR:Au/*p*-Si photodiode were higher than the Co/CR:Au/*n*-Si photodiode. This decrease in RR values with increasing light power confirmed the photodiode behaviors of the devices [33]. The photocurrent values increased almost linearly with increasing light power intensity for both

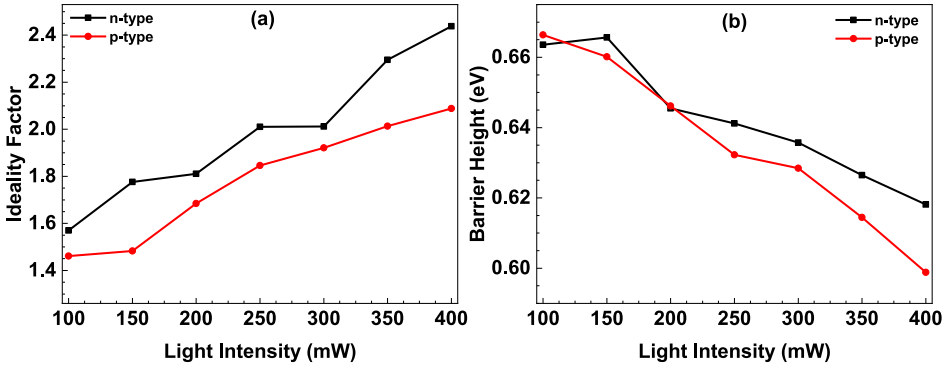

Fig. 5. a) The ideality factor and b) barrier height changes of the Co/CR:Au/*n*-Si and Co/CR:Au/*p*-Si photodiodes, respectively.

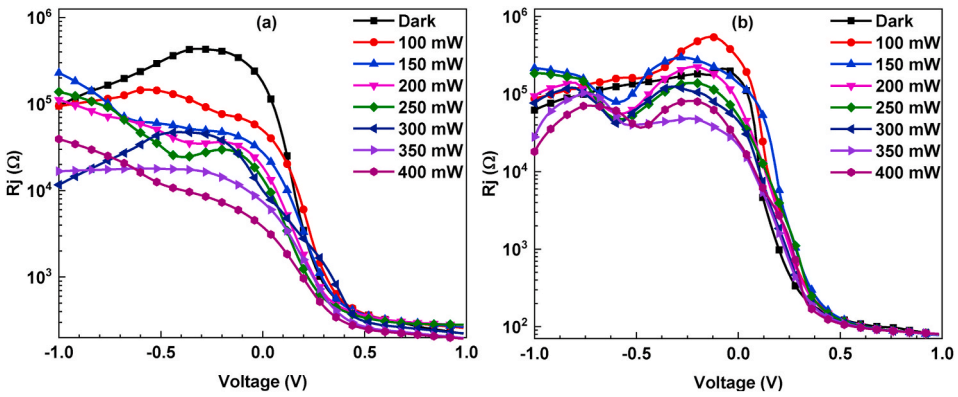

Fig. 6. R_j-V plots of the a) Co/CR:Au/*n*-Si and b) Co/CR:Au/*p*-Si photodiodes for various light illumination power intensities.

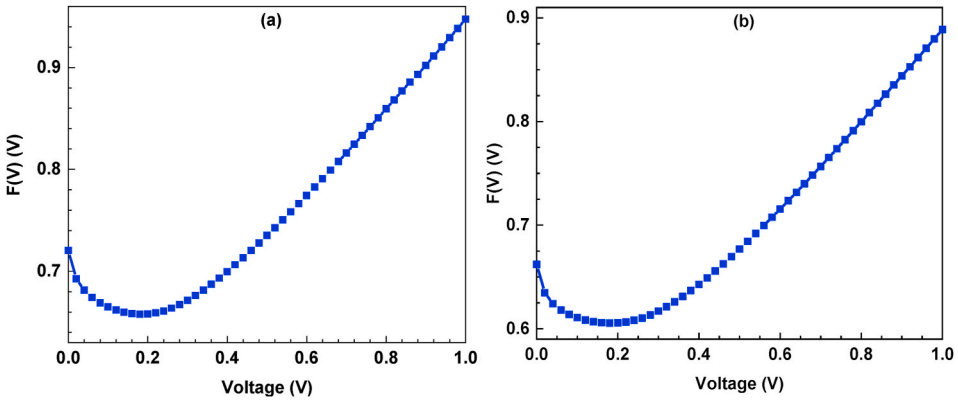

Fig. 7. $F(v)$-V characteristics of the a) Co/CR:Au/*n*-Si and b) Co/CR:Au/*p*-Si photodiodes.

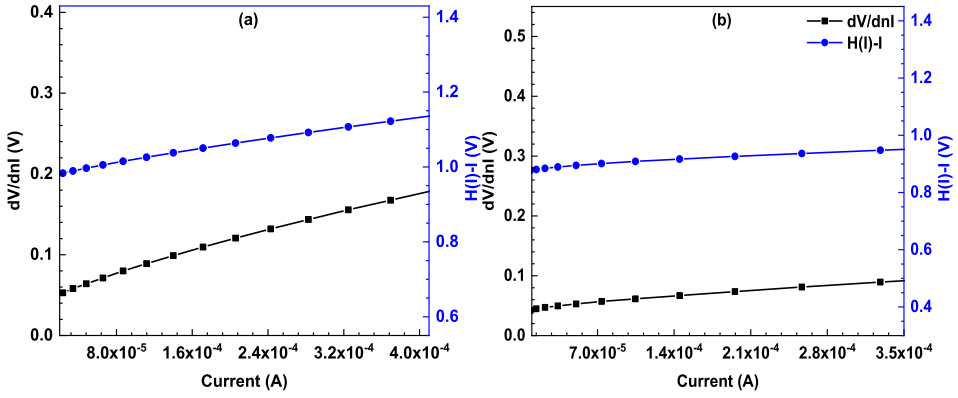

Fig. 8. Cheungs plots of the a) Co/CR:Au/*n*-Si and b) Co/CR:Au/*p*-Si photodiodes.

the Co/CR:Au/*n*-Si and Co/CR:Au/*p*-Si photodiodes at zero bias, but the photocurrent values of the Co/CR:Au/*n*-Si photodiode were slightly higher than those of the Co/CR:Au/*p*-Si photodiode. The responsivity and specific detectivity values of the photodiodes did not change with the increase in the light power intensity. The responsivity and specific detectivity values of the Co/CR:Au/*n*-Si photodiode were higher than those of the Co/CR:Au/*p*-Si photodiode. The photodiodes exhibited good stability with the increase in light power intensity.

4. Conclusion

The Congo red film with Au nanoparticles were formed on both the *n*-Si and *p*-Si substrates by the spin coating technique. UV–Vis spectrometer and TEM were used to determine absorption spectra and surface distribution of the Au nanoparticles on the CR film, respectively. Then, the Co/CR:Au/*n*-Si and Co/CR:Au/*p*-Si devices were fabricated and characterized by *I*–*V* measurements under various light power intensities. Various diode parameters such as ideality factor, barrier height, and series resistance values were calculated and compared for both photodiodes by using different methods. While the ideality factor values increased by increasing light power intensity, the barrier height values decreased. Junction resistance plots revealed that the devices had suitable shunt and series resistance for optoelectronic devices. The responsivity values were higher for the Co/CR:Au/*n*-Si photodiode than for the Co/CR:Au/*p*-Si photodiode. Although the *RR* values decreased with increasing light power intensity, the photocurrent values linearly

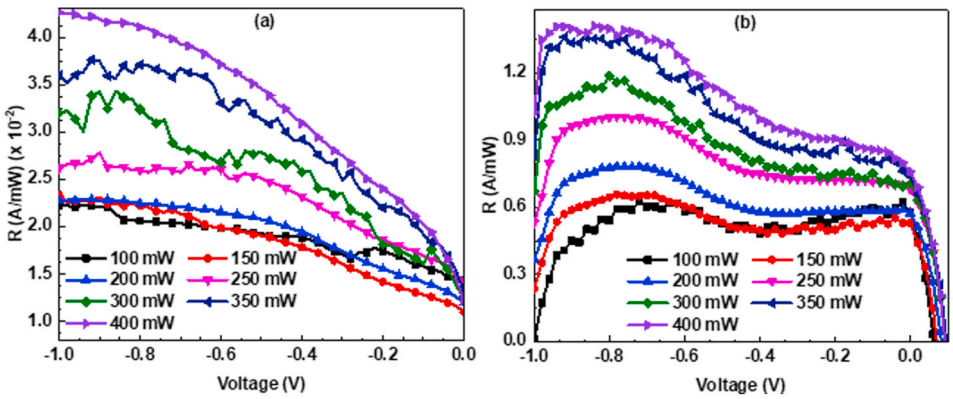

Fig. 9. Responsivity versus voltage plots of the a) Co/CR:Au/*n*-Si and b) Co/CR:Au/*p*-Si photodiodes.

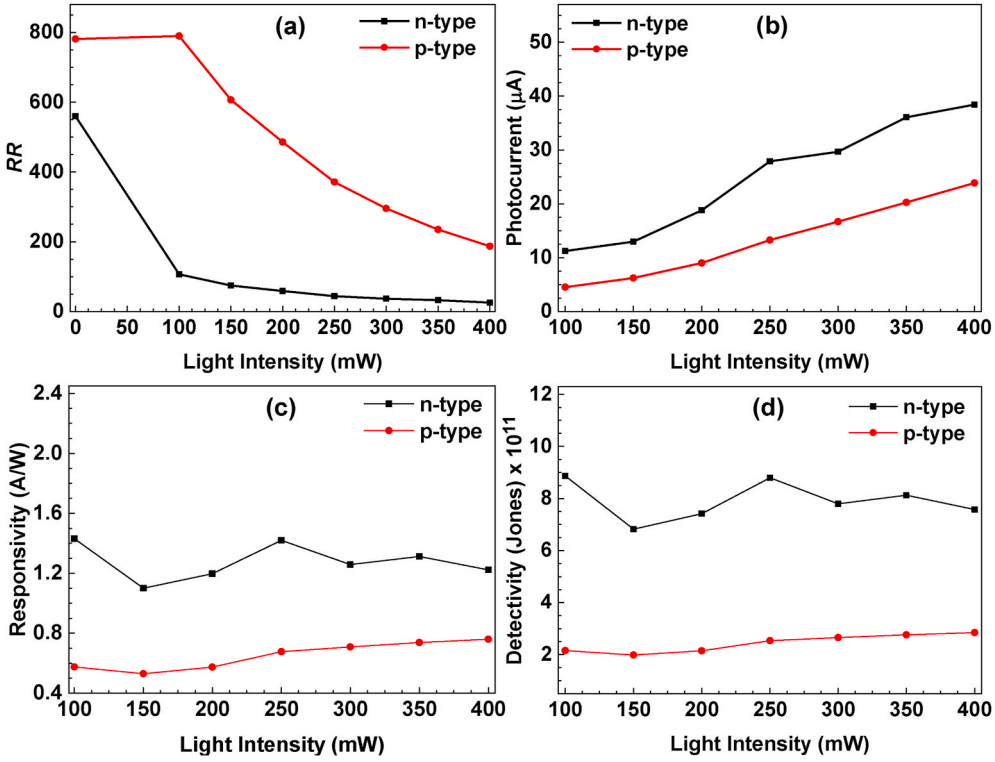

Fig. 10. a) *RR*, b) photocurrent, c) responsivity, and d) detectivity plots of the Co/CR:Au/*n*-Si and Co/CR:Au/*p*-Si photodiodes depending on the changing light power intensity.

increased. According to the photodetector parameters, the fabricated devices can be improved for optoelectronic applications.

Declaration of competing interest

The authors declare that they have no known competing financial interests or personal relationships that could have appeared to influence the work reported in this paper.

References

[1] C.W. Lee, O.Y. Kim, J.Y. Lee, Organic materials for organic electronic devices, J. Ind. Eng. Chem. 20 (2014) 1198–1208, https://doi.org/10.1016/j.jiec.2013.09.036.

[2] Y. Shirota, H. Kageyama, Organic materials for optoelectronic applications: Overview, in: Handb. Org. Mater. Electron. Photonic Devices, Elsevier, 2019, pp. 3–42, https://doi.org/10.1016/b978-0-08-102284-9.00001-2.

[3] H. Li, J.-L. Brédas, Developing molecular-level models for organic field-effect transistors, Natl. Sci. Rev. (2020), https://doi.org/10.1093/nsr/nwaa167.

[4] M. Yilmaz, A. Kocyigit, S. Aydogan, U. Incekara, A. Tursucu, H. Kacus, Light-sensing behaviors of organic/n-Si bio-hybrid photodiodes based on malachite green (MG) organic dye, J. Mater. Sci. Mater. Electron. 31 (2020) 21548–21556, https://doi.org/10.1007/s10854-020-04668-x.

[5] H. Kaçuş, Ç. Çırak, Ş. Aydoğan, Effect of illumination intensity on the characteristics of Co/Congo Red/p-Si/Al hybrid photodiode, Appl. Phys. Mater. Sci. Process 126 (2020) 139, https://doi.org/10.1007/s00339-019-3242-0.

[6] I. Orak, A. Kocyigit, A. Turut, The surface morphology properties and respond illumination impact of ZnO/n-Si photodiode by prepared atomic layer deposition technique, J. Alloys Compd. 691 (2017) 873–879, https://doi.org/10.1016/j.jallcom.2016.08.295.

[7] A. Türüt, Oncurrent-voltage and capacitance-voltage characteristics of metal-semiconductor contacts, Turk. J. Phys. 44 (2020) 302–347, https://doi.org/10.3906/fiz-2007-11.

[8] R.S. Quimby, Photodiode detectors, in: Photonics and Lasers, John Wiley & Sons, Inc., Hoboken, NJ, USA, 2006, pp. 249–279, https://doi.org/10.1002/0471791598.ch14.

[9] A. Ono, Y. Matsuo, H. Satoh, H. Inokawa, Sensitivity improvement of silicon-on-insulator photodiode by gold nanoparticles with substrate bias control, Appl. Phys. Lett. 99 (2011), 062105, https://doi.org/10.1063/1.3622650.

[10] A. Ono, Y. Enomoto, Y. Matsumura, H. Satoh, H. Inokawa, Broadband absorption enhancement of thin SOI photodiode with high-density gold nanoparticles, Opt. Mater. Express 4 (2014) 725, https://doi.org/10.1364/ome.4.000725.
[11] M. Kielar, O. Dhez, G. Pecastaings, A. Curutchet, L. Hirsch, Long-term stable organic photodetectors with ultra low dark currents for high detectivity applications, Sci. Rep. 6 (2016) 1–11, https://doi.org/10.1038/srep39201.
[12] R.D. Jansen-van Vuuren, A. Armin, A.K. Pandey, P.L. Burn, P. Meredith, Organic photodiodes: the future of full color detection and image sensing, Adv. Mater. 28 (2016) 4766–4802, https://doi.org/10.1002/adma.201505405.
[13] H. Kacus, M. Yilmaz, A. Kocyigit, U. Incekara, S. Aydogan, Optoelectronic properties of Co/pentacene/Si MIS heterojunction photodiode, Phys. B Condens. Matter 597 (2020) 412408, https://doi.org/10.1016/j.physb.2020.412408.
[14] A.T. Garcia-Esparza, N. Tymińska, R.A.R. Al Orabi, T. Le Bahers, Full in silico DFT characterization of lanthanum and yttrium based oxynitride semiconductors for solar fuels, J. Mater. Chem. C. 7 (2019) 1612–1621, https://doi.org/10.1039/c8tc05749d.
[15] S.B. Aziz, Morphological and optical characteristics of chitosan(1−x):Cuox ($4 \leq x \leq 12$) based polymer nano-composites: optical dielectric loss as an alternative method for tauc's model, Nanomaterials 7 (2017) 444, https://doi.org/10.3390/nano7120444.
[16] M. Yilmaz, M.L. Grilli, The modification of the characteristics of nanocrystalline ZnO thin films by variation of Ta doping content, Philos. Mag. A 96 (2016) 2125–2142, https://doi.org/10.1080/14786435.2016.1195023.
[17] M. Yilmaz, Ş. Aydoğan, The effect of Pb doping on the characteristic properties of spin coated ZnO thin films: wrinkle structures, Mater. Sci. Semicond. Process. 40 (2015) 162–170, https://doi.org/10.1016/j.mssp.2015.06.064.
[18] M. Yilmaz, A. Kocyigit, B.B. Cirak, H. Kacus, U. Incekara, S. Aydogan, The comparison of Co/hematoxylin/n-Si and Co/hematoxylin/p-Si devices as rectifier for a wide range temperature, Mater. Sci. Semicond. Process. 113 (2020) 105039, https://doi.org/10.1016/j.mssp.2020.105039.
[19] R. Zandonay, R.G. Delatorre, A.A. Pasa, Electrical characterization of electrodeposited Co/p-Si Schottky diodes, ECS Trans., 2008, pp. 359–363, https://doi.org/10.1149/1.2956050.
[20] H. Zhang, Y. Zhao, X. Geng, Y. Huang, Y. Li, H. Liu, Y. Liu, Y. Li, X. Wang, H. Tian, R. Liang, T.L. Ren, Au nanoparticles-decorated surface plasmon enhanced ZnO nanorods ultraviolet photodetector on flexible transparent mica substrate, IEEE J. Electron Devices Soc. 7 (2019) 191–195, https://doi.org/10.1109/JEDS.2018.2889888.
[21] J.D. Hwang, F.H. Wang, C.Y. Kung, M.C. Chan, Using the surface plasmon resonance of Au nanoparticles to enhance ultraviolet response of ZnO nanorods-based Schottky-barrier photodetectors, IEEE Trans. Nanotechnol. 14 (2015) 318–321, https://doi.org/10.1109/TNANO.2015.2393877.
[22] L.B. Luo, X.L. Huang, M.Z. Wang, C. Xie, C.Y. Wu, J.G. Hu, L. Wang, J.A. Huang, The effect of plasmonic nanoparticles on the optoelectronic characteristics of CdTe nanowires, Small 10 (2014) 2645–2652, https://doi.org/10.1002/smll.201303388.
[23] K. Ejderha, N. Yıldırım, B. Abay, A. Turut, Examination by interfacial layer and inhomogeneous barrier height model of temperature-dependent I–V characteristics in Co/p-InP contacts, J. Alloys Compd. 484 (2009) 870–876, https://doi.org/10.1016/J.JALLCOM.2009.05.062.
[24] B. Tatar, A.E. Bulgurcuoglu, P. Gokdemir, P. Aydogan, D. Yilmazer, O. ozdemir, K. Kutlu, Electrical and photovoltaic properties of Cr/Si Schottky diodes, Int. J. Hydrogen Energy 34 (2009) 5208–5212, https://doi.org/10.1016/j.ijhydene.2008.10.040.
[25] A. Kocyigit, M. Yıldırım, A. Sarılmaz, F. Ozel, The Au/Cu2WSe4/p-Si photodiode: electrical and morphological characterization, J. Alloys Compd. 780 (2019) 186–192, https://doi.org/10.1016/j.jallcom.2018.11.372.
[26] L.D. Rao, V.R. Reddy, Electrical parameters and series resistance analysis of Au/Y/p-InP/Pt Schottky barrier diode at room temperature. AIP Conf. Proc., AIP Publishing LLC, 2016, p. 120020, https://doi.org/10.1063/1.4948092.
[27] İ. Taşçıoğlu, W.A. Farooq, R. Turan, Ş. Altındal, F. Yakuphanoglu, Charge transport mechanisms and density of interface traps in MnZnO/p-Si diodes, J. Alloys Compd. 590 (2014) 157–161, https://doi.org/10.1016/J.JALLCOM.2013.12.043.
[28] H. Norde, A modified forward I-V plot for Schottky diodes with high series resistance, J. Appl. Phys. 50 (1979) 5052–5053, https://doi.org/10.1063/1.325607.
[29] S.K. Cheung, N.W. Cheung, Extraction of Schottky diode parameters from forward current-voltage characteristics, Appl. Phys. Lett. 49 (1986) 85, https://doi.org/10.1063/1.97359.
[30] A. Kocyigit, M. Yıldırım, A. Sarılmaz, F. Ozel, The Au/Cu2WSe4/p-Si photodiode: electrical and morphological characterization, J. Alloys Compd. 780 (2019) 186–192, https://doi.org/10.1016/J.JALLCOM.2018.11.372.
[31] H.H. Gullu, D.E. Yildiz, A. Kocyigit, M. Yıldırım, Electrical properties of Al/PCBM: ZnO/p-Si heterojunction for photodiode application, J. Alloys Compd. 827 (2020) 154279, https://doi.org/10.1016/j.jallcom.2020.154279.
[32] G. Luongo, F. Giubileo, L. Genovese, L. Iemmo, N. Martucciello, A. Di Bartolomeo, I-V and C-V characterization of a high-responsivity graphene/silicon photodiode with embedded MOS capacitor, Nanomaterials 7 (2017) 158, https://doi.org/10.3390/nano7070158.
[33] Z. Yuan, A photodiode with high rectification ratio and low turn-on voltage based on ZnO nanoparticles and SubPc planar heterojunction, Phys. E Low-Dimensional Syst. Nanostructures. 56 (2014) 160–164, https://doi.org/10.1016/j.physe.2013.09.001.